Nanoscale

PAPER

Cite this: *Nanoscale*, 2016, **8**, 3085

Etching anisotropy mechanisms lead to morphology-controlled silicon nanoporous structures by metal assisted chemical etching

Bing Jiang,[a] Meicheng Li,*[a,b] Yu Liang,[a] Yang Bai,[c] Dandan Song,[a] Yingfeng Li[a] and Jian Luo*[d]

The etching anisotropy induced by the morphology and rotation of silver particles controls the morphology of silicon nanoporous structures, through various underlying complex etching mechanisms. The level of etching anisotropy can be modulated by controlling the morphology of the silver catalyst to obtain silicon nanoporous structures with straight pores, cone-shaped pores and pyramid-shaped pores. In addition, the structures with helical pores are obtained by taking advantage of the special anisotropic etching, which is induced by the rotation and revolution of silver particles during the etching process. An investigation of the etching anisotropy during metal assisted chemical etching will promote a deep understanding of the chemical etching mechanism of silicon, and provide a feasible approach to fabricate Si nanoporous structures with special morphologies.

Received 21st October 2015,
Accepted 29th December 2015

DOI: 10.1039/c5nr07327h

www.rsc.org/nanoscale

1. Introduction

Nanostructures of silicon (Si), which remains the most important material for the current semiconductor industry, are promising building blocks for devices in the field of nanoelectronics,[1] opto-electronics,[2,3] energy conversion[4–8] and energy storage,[9] as well as bio- and chemical sensors.[10,11] The characteristic parameters of nanostructures, such as surface and cross-section morphologies, orientation relative to the substrate, size and density affect the properties of Si nanostructures and are important for their applications.

Controllable fabrication of Si nanostructures is a prerequisite for their device applications. In recent years, metal-assisted chemical etching (MacEtch) has attracted considerable attention as a facile and cost-effective method for fabricating Si nanostructures with controlled orientation and size features.[12–14] Several prior studies focused on the morphological control of nanoporous Si and Si nanowires through varying the process parameters, such as the oxidant type, etchant concentration, reaction time, processing temperature and type of Si.[15–33] The theory of hole injection during etching is perhaps the most widely accepted mechanism for MacEtch.[4,34–38] Many observations can be qualitatively explained by the holes' injection from noble metal particles as the catalyst into the Si substrate and the subsequent diffusion of holes within the Si substrate. For example, diffusion of positive holes from the bottom to the sidewalls can result in the formation of cone-shaped nanoporous structures and nanowires.[13,18,20]

In previous studies, the Si nanostructures etched by MacEtch were considered to be anisotropic along the <111> and <100> directions. Thus, the etching preferentially took place along the <100> direction to form typical Si nanostructures vertical to the (100) substrate surface, whereas aligned Si nanostructures induced by <100> etching were found on the (111) or (110) substrate surface.[4,5,19,22,25,39] Compared with Si nanowires, the Si nanoporous structures exhibit more diversiform morphologies and their etching mechanisms appear to be more complex. Besides etching anisotropy, sinking of metal particles, shape of metal particles and the distance between the particles also affect the morphology of Si nanoporous structures.[15,31,34,40] However, the exact formation mechanisms of various Si nanoporous structures, including helical, square and cone-shaped pores, are not well explained. The effects of the movement of metal particles on the formation of Si nanoporous structures remain elusive. Thus, the scientific goal of this paper is to clarify related etching mechanisms *via* fabricating various Si nanoporous structures by systematically varying several key processing parameters to subsequently achieve mechanism-informed morphological control of Si nanoporous structures.

[a]*State Key Laboratory of Alternate Electrical Power System with Renewable Energy Sources, North China Electric Power University, Beijing 102206, China. E-mail: mcli@ncepu.edu.cn, jluo@alum.mit.edu; Fax: +86-10-61772951*
[b]*Suzhou Institute, North China Electric Power University, Suzhou 215123, China*
[c]*Corrosion and Protection Center, Key Laboratory for Environmental Fracture (Ministry of Education), University of Science and Technology Beijing, Beijing 100083, China*
[d]*Department of NanoEngineering, Program of Materials Science and Engineering University of California, San Diego, La Jolla, CA 92093, USA*

2. Experimental details

p-Type Si (100) single crystal wafers with a resistivity of $\rho \sim$ 7–13 Ω cm were purchased from Emei Semiconductor Factory, China. Single-side polished Si wafers were cut into 1.5 cm × 1.0 cm pieces. Silver nitrate ($AgNO_3$), aqueous ammonia ($NH_3{\cdot}H_2O$), glucose ($CH_2OH(CHOH)_4CHO$), hydrofluoric acid (HF, 40%) and hydrogen peroxide (H_2O_2, 30%) were purchased from Sinopharm Chemical Reagent Beijing Company. All the chemicals were reagent grade and deionized water was used to prepare the aqueous solutions of desired concentrations.

The Si samples were cleaned by sonicating in solutions of 40% HF and deionized water. $AgNO_3$ powders were dissolved in a solvent composed of water and ethanol to prepare $AgNO_3$ solutions. $NH_3{\cdot}H_2O$ (0.3 M) was continuously dripped into the $AgNO_3$ solution while stirring until the solution became colorless. The 0.2 M $[Ag(NH_3)_2]OH$ solution was prepared by mixing appropriate amounts of $AgNO_3$ and $NH_3{\cdot}H_2O$ solutions. Then, the cleaned and dried Si samples were placed into the $[Ag(NH_3)_2]OH$ aqueous solution, where the oxidizing $[Ag(NH_3)_2]^+$ was reduced to Ag particles by glucose (0.05 M) and deposited on the Si surface *via* the well-known silver mirror reaction. The morphology of Ag particles on the Si surface can be controlled by the reaction temperature.[41] In this experiment, isolated Ag particles were deposited on the Si substrate *via* a room-temperature reaction for 5 minutes, while continuous layers of Ag particles were prepared on the Si surfaces by a reaction at 60 °C for 3 minutes.

The isolated Ag particles and continuous Ag layers on Si surfaces were used as catalysts to etch Si nanostructures. The etchant solutions are comprised of HF, H_2O_2 and H_2O. Different Si nanoporous structures were obtained by systematically varying the etching times (5 min, 30 min, 1 h, 2 h and 4 h), and the concentration of the etchant ($1HF : 5H_2O_2 : 10 H_2O$, $1HF : 5H_2O_2 : 2H_2O$, which are referred to as dilute and concentrated etching solutions in the following text). Moreover, the isolated Ag particles were used to prepare the helical pores. Then, the formation mechanism of Si helical pores was also investigated by controlling the concentration of HF (40%–90%) (either in dilute or concentrated solutions). The surface and cross-section morphologies of Si pores were characterized by using a scanning electron microscope (SEM, FEI Quanta 200F).

3. Results and discussion

3.1 Etching anisotropy induced by Ag morphology

Previous studies show that the etching of Si is intrinsically anisotropic, which can be explained by the back-bond breaking theory.[4,34] Due to the different back-bond strengths, it is easier to remove Si atoms on the (100) surface planes, thus, etching occurs preferentially along the <100> direction. The vertical nanowires along the <100> direction on the (100) Si surface and the inclined nanowires along the <100> direction on the (111) or (110) Si surfaces were evident in previous studies.[5,25] In our experiments, various Si nanoporous structures are obtained through using either isolated particles or continuous layers of Ag as catalyst whether in dilute or concentrated etching solutions. Fig. 1(a)–(c) show isolated Ag particles deposited on the Si surface and the corresponding Si nanoporous structures that are made using them as catalysts in a dilute

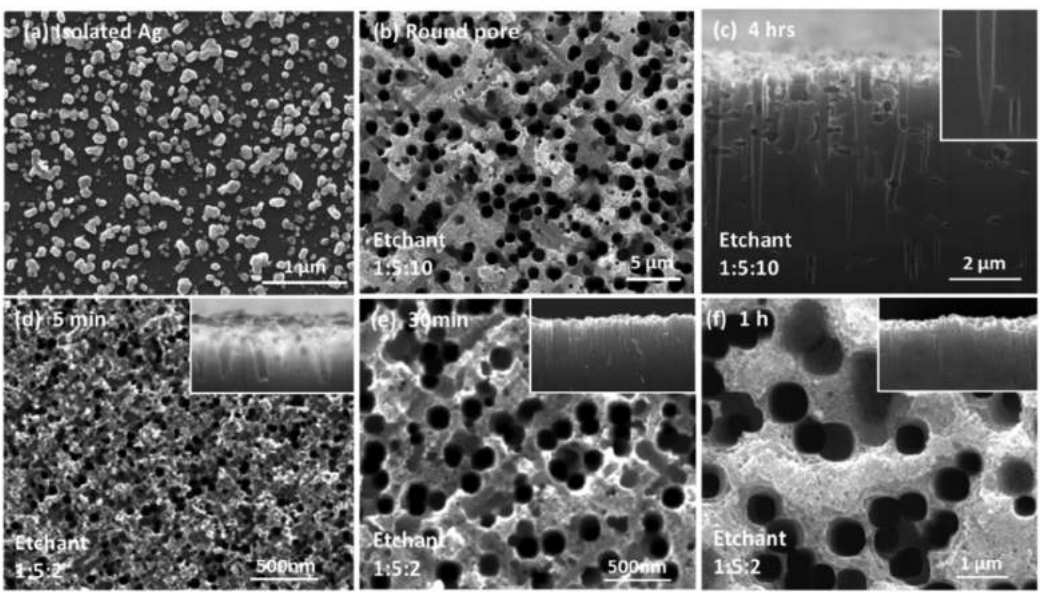

Fig. 1 SEM micrographs of (a) isolated Ag catalyst particles on the surface of a Si wafer and (b) the Si nanoporous structure obtained after etching in a dilute $1HF : 5H_2O_2 : 10H_2O$ solution for 4 hours and (c) the corresponding cross-section morphology; (d) the Si nanoporous structure obtained after etching in a concentrated $1HF : 5H_2O_2 : 2H_2O$ solution for 5 min, (e) 30 min and (f) 1 hour. The insets show the corresponding cross-section of the pores.

etching solution ($1HF : 5H_2O_2 : 10H_2O$). Deep straight pores form after a long etching time of 4 hours, which are typical anisotropic etching structures along the <100> direction. Using a concentrated etching solution ($1HF : 5H_2O_2 : 2H_2O$), similar pores are obtained by isolated Ag particles as the catalyst. Fig. 1(d) and (e) illustrate that still straight pores form and their sizes and depths increase with increasing etching time. Under these conditions, the etching rate is about four times that when the dilute etching solution is used.

Under the same etching conditions, an ~1 μm-thick, and flocculent, continuous layer of Ag catalyst is used to make Si nanoporous structures, as shown in Fig. 2(a). Fig. 2(b) and (c) show that quasi-square cone pores with rough sidewalls are obtained in the diluted solution. The rough sidewalls in the cross-section image correspond to the stripes in the top view image, as shown in Fig. 2(d) and (e). However, in the concentrated solution, cone-shaped and pyramid-shaped pores and porous craters are obtained by applying continuous Ag layers, as shown in Fig. 3.

From the results it can be seen that the different Si nanoporous structures likely result from the different morphologies of the catalytic Ag particles whether in a dilute or in a concentrated solution. The deep straight pores are obtained by using isolated Ag particles as the catalyst whereas quasi-square cone-shaped pores and inverted pyramid-shaped pores are etched by using continuous Ag layers. The isolated Ag particles have a higher catalytic activity than that of the continuous layers due to the fact that isolated Ag particles are smaller and easier to move around. Therefore, most pores etched by isolated Ag particles are vertical straight pores along the <100> direction because of the drastic etching anisotropy due to the high catalytic activity of Ag particles, as shown in Fig. 1(b) and (c). In the concentrated solution, the combination of the high etching rate and the small size of isolated Ag particles drastically intensifies the anisotropic etching, with fast etching along the <100> direction to form straight pores, as shown in Fig. 1(d)–(f). However, when continuous Ag layers are used as catalysts, the difference in etching between the <100> and <111> directions can be observed because of the appropriate catalytic activity due to the continuous morphology of the Ag layer. Comparing Fig. 1(a) and 2(a), it is evident that the Ag particles in the continuous layer are bigger and denser, and they presumably have lower mobility. Therefore, the etching anisotropy is weakened significantly due to the low catalytic activity of continuous Ag layers. In Fig. 2(d), multiple stripes (screw lines) are observed on the sidewalls of the pores, which are likely the footprints left by the rotating Ag particles. Thus, it is considered that the different Si nanoporous structures are ascribed to not only etching anisotropy but also to the movement of Ag particles during etching. Fig. 3(a) shows inverted pyramid-shaped pores that are obtained in a concentrated solution, as a result of anisotropic etching between <100> and <111> directions due to facet etching (Ag layer) instead of point etching (isolated Ag). The four edges of an inverted pyramid are induced by preferential etching along the <100> directions, whereas the four triangle facets originate from etching along the <111> directions, as depicted in Fig. 3(b). With increasing etching time, Ag particles in the continuous

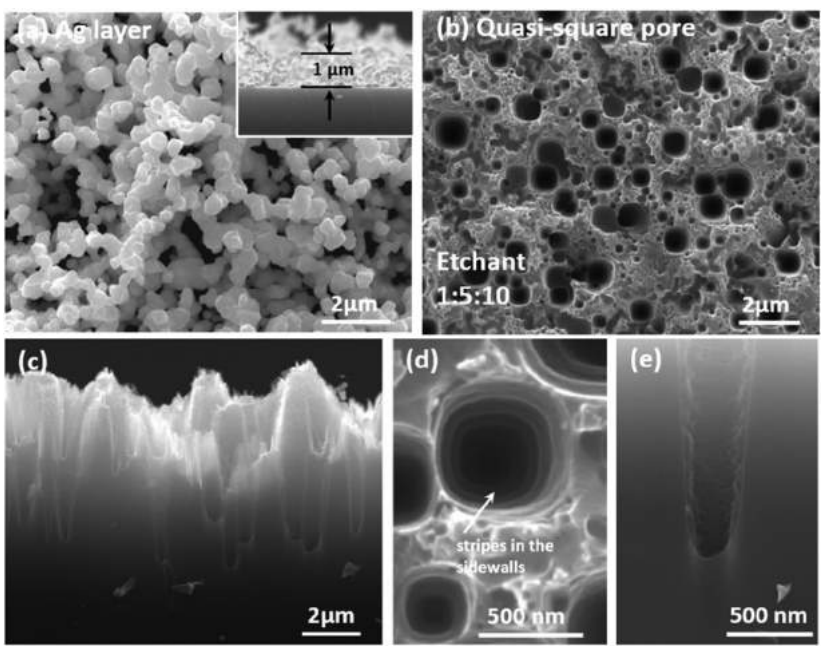

Fig. 2 SEM micrographs of (a) a continuous layer of Ag catalyst and (b) the Si quasi-square, cone-shaped pores obtained after etching in a dilute $1HF : 5H_2O_2 : 10H_2O$ solution for 4 hours using the catalyst shown in panel (a). Additional SEM micrographs of (c) a cross-section of the Si nanoporous structure, (d) an enlarged view of quasi-square pores with screw lines on the insight surface, and (e) a cross-section showing that the pore has a cone shape with a rough surface.

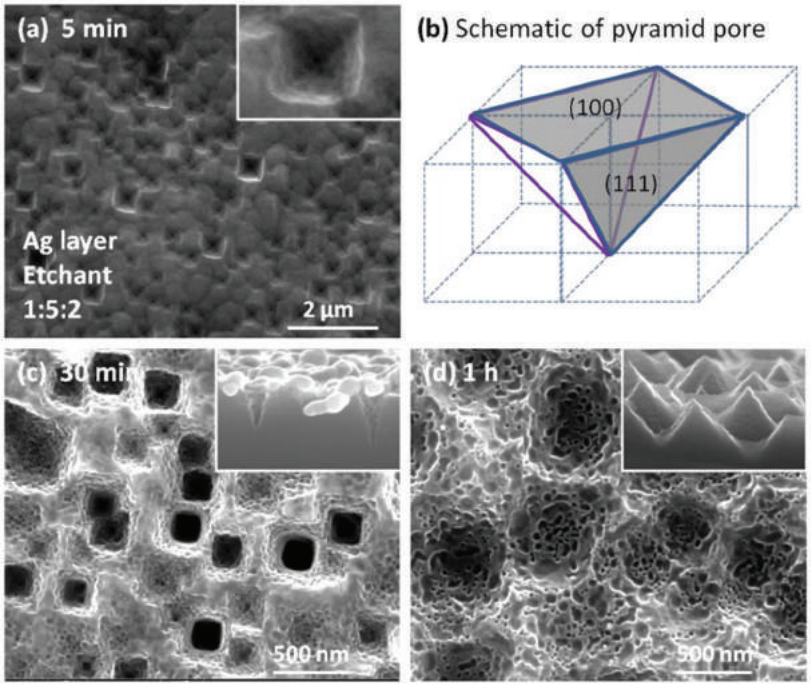

Fig. 3 SEM micrographs of the square pyramid-shaped pores etched in a concentrated 1HF : $5H_2O_2$: $2H_2O$ solution using continuous layers of Ag catalyst particles for (a) 5 minutes, (c) 30 minutes, and (d) 1 hour, respectively. The insets are the corresponding cross-sectional morphologies. A schematic of the inverted pyramid pore is shown in (b).

layer partially break loose and sink into the Si substrate to drill pores, and the base of the pores remains square-shaped but their cross-section becomes cone-shaped, as shown in Fig. 3(c). The Si surface is severely etched after 1 hour to become a porous crater structure, as shown in Fig. 3(d), which presumably resulted from a secondary etching process (from the subsequent Ag particles that break off from the continuous layer). From the above results, the morphology of the Si nanoporous structure is determined by the etching anisotropy and mobility of the Ag particles. The level of etching anisotropy is different when the Ag particles or layers with different morphologies are used as catalysts.

3.2 The rotation of Ag particles for helical pores

In previous studies, helical pores were observed under special etching conditions and could be reduced or eliminated by varying the concentration of the oxidant in the etchant,[25] which could presumably result from the anisotropic etching rate.[40] In our studies, we observed helical pores with different cross-sectional morphologies for the case where isolated Ag particles are used as catalysts in the etching solution with different HF concentrations. By contrast, when the Ag layer is used as a catalyst, helical pores cannot be obtained, but some cone-shaped or pyramid-shaped pores are obtained. Therefore, the helical pores are ascribed to the movement of isolated Ag particles. The underlying mechanisms for forming helical pores *via* the various modes of coupled particle rotation, revolution, and etching anisotropy are discussed in detail.

Fig. 4 shows helical pores with different pitches and shapes, the formation of which is related to the concentration of HF. It is found that 40% is the critical ratio of HF between the straight pores and helical pores. Straight pores are obtained when the ratio of HF is lower than 40% (see Fig. 4(a)). On increasing the ratio of HF above 40%, the helical shape of the pores is more obvious, in which the pitch and width of pores change, as shown in Fig. 4(b)–(h). Moreover, it can be seen from Fig. 4(d) that there are stripes in the sidewalls of pores in the top view. In the literature, the catalytic activity of metal particles is anisotropic (on a different facet), which is determined by the shape of Ag particles.[15,17,20,31,40] The helical pore was attributed to the microscopic difference in the etching rate of Si on the Pt particles.[40] Meanwhile, spherical Ag particles are observed in the bottom of pores, which is explained by the dissolution of Ag particles in the etching process.[15,40] Therefore, the anisotropy should be decreased by spherical Ag particles due to dissolution in the later etching process. In our studies, the etching anisotropy induced by the moving path of Ag particles during etching, as a possible mechanism, is proposed to explain the formation of various helical pores. In a relevant mass transfer model for etching, it is proposed that the Si atoms are oxidized and dissolved at the interface between the metal particles and the Si substrate, and the reagent and the byproduct diffuse along this interface.[34] This mechanism is supported by Liu *et al.*'s etching experiments using anisotropic Pt nanoparticles as catalysts.[31] Under a lower HF concentration, the Si/Ag interface

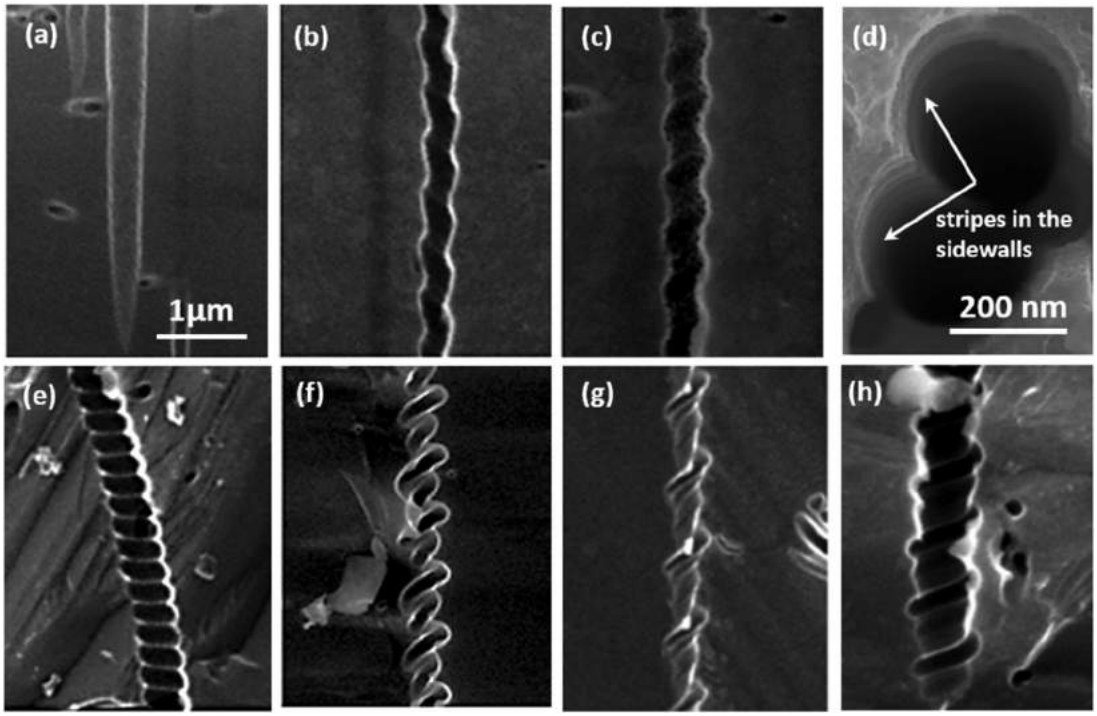

Fig. 4 Cross-sectional SEM micrographs of helical pores with different morphologies etched by isolated Ag particles. (a) 16.7% HF (b) and (c) 40% HF (d) an enlarged top view of helical pores under 50% HF (e) 50% HF (f) 83.3% HF (g) and (h) 90% HF.

may be covered with a silicon oxide layer. In this case, the movement of Ag particles is relatively stable and the Si surface can be uniformly etched by positive holes and can generate deep straight pores (see Fig. 4(a)). However, in solutions with a high HF concentration, the oxide layer formed at the Si/Ag interface is thin and easily damaged because the oxide is dissolved at a fast rate. That is, oxidation and dissolution occur simultaneously. Because of the strong interactions at the Si/Ag interface, the non-uniform etching at the Si/Ag interface leads to the Ag particles being under an unbalanced surface stress. Moreover, according to the typical anode reaction model, hydrogen could be produced at the interface between Si and Ag particles.[34] In the current experiments, we observed that the samples move around in the etchant when hydrogen is bubbling out from the Si surface during the etching procedures. Due to gravity, surface stress and flowing of hydrogen and the reagent, the Ag particles could rotate during the etching procedure. In particular, the rotation direction of Ag particles determines the moving path resulting in different morphological helical pores. Fig. 5 illustrates the relationship between the rotation direction of Ag particles and the morphology of different helical pores. When the angle θ is small, the pitch length of the resultant helical pore will be small, as shown in Fig. 5(b). Moreover, all helical pores are found to have internal stripes (screw lines) on their inside sidewalls, which suggests that Ag particles rotate and etch against the inside sidewalls of the pores during the etching and sinking processes, as shown in Fig. 4(d). Whether in concentrated or dilute solutions, only the concentration of HF is the key factor for the formation of helical pores, resulting in reaction activities at the interface of Ag particles and the Si surface.

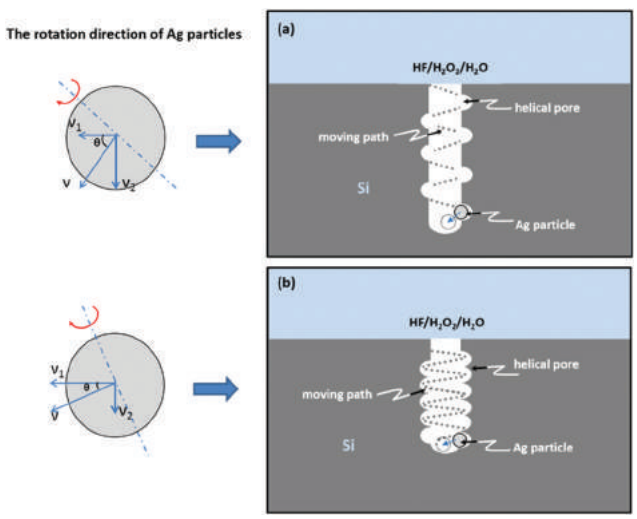

Fig. 5 Schematic illustration of the rotational direction and probable moving paths of Ag particles and during the process of forming helical pores with different pitches and widths.

Some complex helical pores are also observed in our experiments. Fig. 6(a) shows that several Ag particles gather together

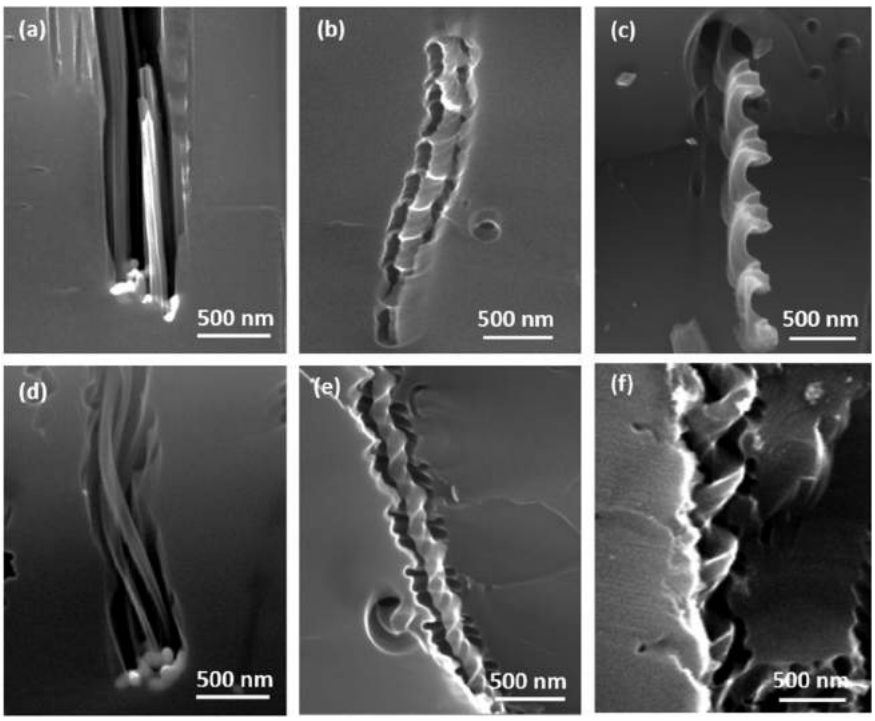

Fig. 6 Cross-sectional SEM micrographs of several helical pores with complex morphologies. (a, d) entangled multiple pores; (b, e) helical pores with the screw-line Si pillar in the centers; (c, f) helical bent nanowires detached from the pores.

under the bottom of a complex helical pore with a large pitch length (HF >40%). When several Ag particles are close to each other, they appear to move in a coordinated path (presumably through the interactions of the stress field) forming this complex, multi-trace, helical pore. However, when the ratio of HF is lower than 40%, these kinds of multi-trace pores are not helical even though the Ag particles can also move in a coordinated fashion, as shown in Fig. 6(d). Moreover, unique helical pores with Si pillars in the center of the pores are observed, and two examples are shown in Fig. 6(b) and (e). These pores could be induced by the simultaneous rotation and revolution of Ag particles during the etching procedure, and the hypothesized etching process is schematically illustrated in Fig. 7. This model shows that when the radius of revolution is larger than the radius of the Ag particles, a Si pillar can remain in the center of the pore (see Fig. 7(b)). The paths of revolution of Ag particles are clearly evident from spiral stripes in the Si pillars, as shown in Fig. 6(b) and (e). The revolution and rotation of Ag particles should be driven by the hydrodynamics in etchant solutions. When these Si pore structures are further etched, detached helical nanowires are observed, as shown in Fig. 6(c) and (f).

From the above results about helical pores, it is proposed that the rotation and revolution of Ag particles play an impor-

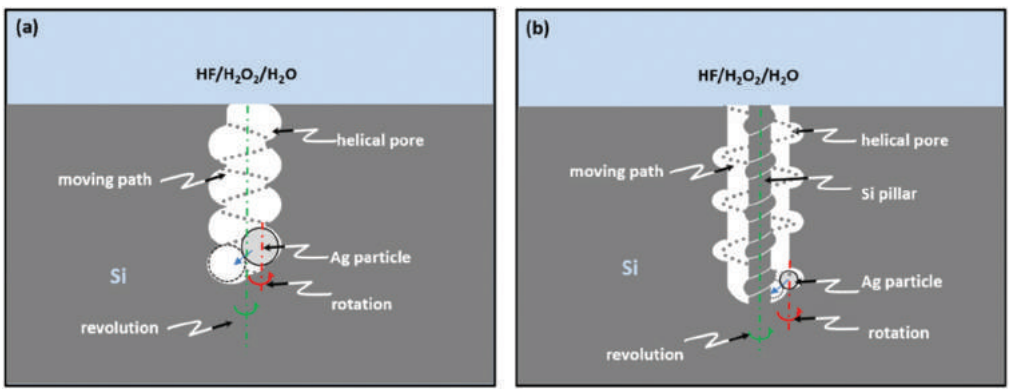

Fig. 7 Schematic illustrations of the formation of (a) normal helical pores and (b) helical pores with the screw-line Si pillar in the center.

tant role in the formation of various helical Si nanoporous structures. Therefore, the various helical pores originate from the concentration of HF, which can induce the rotation and revolution of Ag particles inside the pores during the etching process. In fact, the helical pore can be thought to come from another etching anisotropy induce by rotation and revolution of Ag particles.

4. Conclusions

In summary, the morphological control of silicon nanoporous structures has been achieved by a systematic utilization of etching anisotropy in the process of metal assisted chemical etching. The straight deep pores are obtained by isolated Ag particles, whereas the quasi-square and pyramid-shaped pores are induced by continuous Ag layers, which are determined by the different levels of etching anisotropy. The helical pores form as a result of the rotation of Ag particles under a higher HF concentration (>40%). The helical pores with several more complex morphologies, such as entangled multiple spiral pores and helical pores with Si pillars with screw-lines, are ascribed to the revolution of Ag particles. The formation of Si helical pores is regarded as another anisotropic etching induced by the rotation or revolution of Ag particles. This study demonstrates the feasibility of fabricating the Si porous structures of various morphologies *via* regulating the etching anisotropy by the morphology and movement of catalytic Ag particles.

Acknowledgements

This work was supported partially by National High-tech R&D Program of China (863 Program, No. 2015AA034601), National Natural Science Foundation of China (Grant No. 91333122, 51402106, 51372082, 51172069, 51202067 and 61204064), Ph. D. Programs Foundation of Ministry of Education of China (Grant No. 20120036120006, 20130036110012), Par-Eu Scholars Program, Fundamental Research Funds for the Central Universities, and China Scholarship Council. J. Luo also acknowledges partial support from a NSSEFF fellowship (ONR Grant No. N00014-15-1-0030).

References

1 V. Schmidt, H. Riel, S. Senz, S. Karg, W. Riess and U. Gösele, *Small*, 2006, **2**, 85–88.
2 B. Tian, X. Zheng, T. J. Kempa, Y. Fang, N. Yu, G. Yu, *et al.*, *Nature*, 2007, **449**, 885–889.
3 F. Bai, M. Li, P. Fu, R. Li, T. Gu, R. Huang, *et al.*, *APL Mater.*, 2015, **3**, 056101.
4 K. Peng, A. Lu, R. Zhang and S.-T. Lee, *Adv. Funct. Mater.*, 2008, **18**, 3026–3035.
5 Z. Huang, T. Shimizu, S. Senz, Z. Zhang, X. Zhang, W. Lee, *et al.*, *Nano Lett.*, 2009, **9**, 2519–2525.
6 F. Hui, L. Xudong, S. Shuang, X. Ying and Z. Jing, *Nanotechnology*, 2008, **19**, 255703.
7 D. Kumar, S. K. Srivastava, P. K. Singh, M. Husain and V. Kumar, *Sol. Energy Mater. Sol. Cells*, 2011, **95**, 215–218.
8 F. Bai, M. Li, D. Song, H. Yu, B. Jiang and Y. Li, *J. Solid State Chem.*, 2012, **196**, 596–600.
9 K. Q. Peng, J. S. Jie, W. J. Zhang and S. T. Lee, *Appl. Phys. Lett.*, 2008, 93.
10 Y. Cui, Q. Wei, H. Park and C. M. Lieber, *Science*, 2001, **293**, 1289–1292.
11 F. Patolsky, G. Zheng and C. M. Lieber, *Nat. Protoc.*, 2006, **1**, 1711–1724.
12 X. Li and P. W. Bohn, *Appl. Phys. Lett.*, 2000, **77**, 2572–2574.
13 F. Bai, M. Li, R. Huang, Y. Li, M. Trevor and K. P. Musselman, *RSC Adv.*, 2014, **4**, 1794–1798.
14 F. Bai, M. Li, R. Huang, Y. Yu, T. Gu, Z. Chen, *et al.*, *J. Nanopart. Res.*, 2013, 15.
15 K. Tsujino and M. Matsumura, *Adv. Mater.*, 2005, **17**, 1045–1047.
16 D. C. Lim, I. Lopez-Salido and Y. D. Kim, *Appl. Surf. Sci.*, 2006, **253**, 959–965.
17 K. Tsujino and M. Matsumura, *Electrochim. Acta*, 2007, **53**, 28–34.
18 C. Chartier, S. Bastide and C. Lévy-Clément, *Electrochim. Acta*, 2008, **53**, 5509–5516.
19 C.-Y. Chen, C.-S. Wu, C.-J. Chou and T.-J. Yen, *Adv. Mater.*, 2008, **20**, 3811–3815.
20 C.-L. Lee, K. Tsujino, Y. Kanda, S. Ikeda and M. Matsumura, *J. Mater. Chem.*, 2008, **18**, 1015–1020.
21 Y. M. Yang, P. K. Chu, Z. W. Wu, S. H. Pu, T. F. Hung, K. F. Huo, *et al.*, *Appl. Surf. Sci.*, 2008, **254**, 3061–3066.
22 M.-L. Zhang, K.-Q. Peng, X. Fan, J.-S. Jie, R.-Q. Zhang, S.-T. Lee, *et al.*, *J. Phys. Chem. C*, 2008, **112**, 4444–4450.
23 O. J. Hildreth, W. Lin and C. P. Wong, *ACS Nano*, 2009, **3**, 4033–4042.
24 M. L. Chourou, K. Fukami, T. Sakka, S. Virtanen and Y. H. Ogata, *Electrochim. Acta*, 2010, **55**, 903–912.
25 Z. Huang, T. Shimizu, S. Senz, Z. Zhang, N. Geyer and U. Gösele, *J. Phys. Chem. C*, 2010, **114**, 10683–10690.
26 X. Geng, M. Li, L. Zhao and P. W. Bohn, *J. Electron. Mater.*, 2011, **40**, 2480–2485.
27 S.-C. Shiu, S.-B. Lin, S.-C. Hung and C.-F. Lin, *Appl. Surf. Sci.*, 2011, **257**, 1829–1834.
28 S. Yae, Y. Morii, N. Fukumuro and H. Matsuda, *Nanoscale Res. Lett.*, 2012, **7**, 352–358.
29 J. Cichoszewski, M. Reuter, F. Schwerdt and J. H. Werner, *Electrochim. Acta*, 2013, **109**, 333–339.
30 N. Geyer, B. Fuhrmann, H. S. Leipner and P. Werner, *ACS Appl. Mater. Interfaces*, 2013, **5**, 4302–4308.
31 G. Liu, K. L. Young, X. Liao, M. L. Personick and C. A. Mirkin, *J. Am. Chem. Soc.*, 2013, **135**, 12196–12199.
32 A. Backes and U. Schmid, *Sens. Actuators, B*, 2014, **193**, 883–887.
33 F. Bai, M. Li, R. Huang, D. Song, B. Jiang and Y. Li, *Nanoscale Res. Lett.*, 2012, **7**, 1–5.

34 Z. Huang, N. Geyer, P. Werner, J. de Boor and U. Gosele, *Adv. Mater.*, 2011, **23**, 285–308.
35 C.-Y. Chen and C.-P. Wong, *Chem. Commun.*, 2013, **49**, 7295–7297.
36 C. Q. Lai, H. Cheng, W. K. Choi and C. V. Thompson, *J. Phys. Chem. C*, 2013, **117**, 20802–20809.
37 Z. R. Smith, R. L. Smith and S. D. Collins, *Electrochim. Acta*, 2013, **92**, 139–147.
38 R. Douani, K. Si-Larbi, T. Hadjersi, N. Megouda and A. Manseri, *Phys. Status Solidi A*, 2008, **205**, 225–230.
39 H. Chen, H. Wang, X.-H. Zhang, C.-S. Lee and S.-T. Lee, *Nano Lett.*, 2010, **10**, 864–868.
40 K. Tsujino and M. Matsumura, *Electrochem. Solid-State Lett.*, 2005, **8**, C193.
41 B. Jiang, M. Li, D. Song, Y. Li and T. Mwenya, *Cryst. Res. Technol.*, 2013, **48**, 1044–1049.